Electronic Supplementary Material (ESI) for RSC Advances.
This journal is © The Royal Society of Chemistry 2015

Supporting Information

Fine-tuning of the dielectric properties of polysiloxanes by chemical modification

Simon J. Dünki,[1,2] Martin Tress,[3] Friedrich Kremer,[3]* Song Yee Ko,[1,2] Frank A. Nüesch,[1,2] Cristian-Dragos Varganici,[4] Carmen Racles,[4] Dorina M. Opris[1]*

P2: ^{1}H NMR ($CDCl_3$, δ): 2.60 – 2.48 (m, 4H, -C<u>H</u>$_2$-S-C<u>H</u>$_2$-), 1.60 – 1.52 (m, 2H, C<u>H</u>$_2$-CH_2-CH_3), 1.46 – 1.37 (m, 2H, C<u>H</u>$_2$-CH_3), 0.94 – 0.87 (m, 5H, Si-C<u>H</u>$_2$-, CH_2-C<u>H</u>$_3$). 0.14 (s, 3H, Si-C<u>H</u>$_3$); ^{13}C NMR ($CDCl_3$, δ): 31.9, 31.8, 22.2, 18.5, 13.9, 0.1; ^{29}Si NMR ($CDCl_3$, δ) 24.0; EA: Calcd.: C 47.68, H 9.14, S 18.18; found C 47.56, H 9.11, S 17.95.

P2$_9$P3$_1$: ^{1}H NMR ($CDCl_3$, δ): 2.83 – 2.78 (m, 2H, C<u>H</u>$_2$-CH_2-CN), 2.69 – 2.62 (m, 4H, C<u>H</u>$_2$-S-CH_2-C<u>H</u>$_2$-CN), 2.59 – 2.49 (m, 36H, C<u>H</u>$_2$-S-C<u>H</u>$_2$-Pr), 1.61 –1.52 (m, 18H, C<u>H</u>$_2$-CH_2-CH_3), 1.46 – 1.36 (m, 18H, C<u>H</u>$_2$-CH_3), 0.95 – 0.86 (m, 47H, Si-C<u>H</u>$_2$-, CH_2-C<u>H</u>$_3$). 0.14 (s, 30H, Si-C<u>H</u>$_3$); ^{13}C NMR ($CDCl_3$, δ): 118.4, 31.82, 31.76, 27.7, 26.8, 26.5, 22.2, 19.0, 18.4, 18.2, 13.8, 0.0; ^{29}Si NMR ($CDCl_3$, δ) 24.0; EA: Calcd.: C 47.08, H 8.87, N 0.8, S 18.21; found: C 48.42, H 8.72, N 1.62, S 17.78.

P2$_8$P3$_2$: ^{1}H NMR ($CDCl_3$, δ): 2.83 – 2.77 (m, 4H, C<u>H</u>$_2$-CH_2-CN), 2.69 – 2.62 (m, 8H, C<u>H</u>$_2$-S-CH_2-C<u>H</u>$_2$-CN), 2.59 – 2.49 (m, 32H, C<u>H</u>$_2$-S-C<u>H</u>$_2$-Pr), 1.60 –1.51 (m, 16H, C<u>H</u>$_2$-CH_2-CH_3), 1.45 – 1.35 (m, 16H, C<u>H</u>$_2$-CH_3), 0.95 – 0.85 (m, 44H, Si-C<u>H</u>$_2$-, CH_2-C<u>H</u>$_3$). 0.14 (s, 30H, Si-C<u>H</u>$_3$); ^{13}C NMR ($CDCl_3$, δ): 118.5, 31.84, 31.77, 27.7, 26.8, 26.5, 22.2, 19.0, 18.5, 18.2, 13.8, 0.1; ^{29}Si NMR ($CDCl_3$, δ): 24.0; EA: Calcd.: C 46.47, H 8.60, N 1.59, S 18.25; found: C 46.23, H 8.84, N 1.65, S 18.05.

P2$_7$P3$_3$: ^{1}H NMR ($CDCl_3$, δ): 2.84 – 2.77 (m, 6H, C<u>H</u>$_2$-CH_2-CN), 2.70 – 2.62 (m, 12H, C<u>H</u>$_2$-S-CH_2-C<u>H</u>$_2$-CN), 2.58 – 2.47 (m, 28H, C<u>H</u>$_2$-S-C<u>H</u>$_2$-Pr), 1.60 –1.51 (m, 14H, C<u>H</u>$_2$-CH_2-CH_3),

1.46 – 1.35 (m, 14H, C$\underline{H}_2$-CH_3), 0.96 – 0.85 (m, 41H, Si-C$\underline{H}_2$-, CH_2-C$\underline{H}_3$). 0.14 (s, 30H, Si-C$\underline{H}_3$); ^{13}C NMR ($CDCl_3$, δ): 118.5, 31.86, 31.78, 27.7, 26.9, 26.5, 22.2, 19.1, 18.5, 18.2, 13.9, 0.1; ^{29}Si NMR ($CDCl_3$, δ): 24.6, 23.8; EA: Calcd.: C 45.87, H 8.33, N 2.40, S 18.28; found: C 45.71, H 8.48, N 2.46, S 17.99.

P2$_6$P3$_4$: ^{1}H NMR ($CDCl_3$, δ): 2.85 – 2.77 (m, 8H, C$\underline{H}_2$-CH_2-CN), 2.70 – 2.61 (m, 16H, C$\underline{H}_2$-S-CH_2-C$\underline{H}_2$-CN), 2.58 – 2.48 (m, 24H, C$\underline{H}_2$-S-C$\underline{H}_2$-Pr), 1.60 –1.51 (m, 12H, C$\underline{H}_2$-CH_2-CH_3), 1.46 – 1.35 (m, 12H, C$\underline{H}_2$-CH_3), 0.97 – 0.85 (m, 38H, Si-C$\underline{H}_2$-, CH_2-C$\underline{H}_3$). 0.14 (s, 30H, Si-C$\underline{H}_3$); ^{13}C NMR ($CDCl_3$, δ): 118.6, 31.9, 31.8, 27.7, 26.8, 26.5, 22.2, 19.1, 18.4, 18.2, 13.8, 0.1; ^{29}Si NMR ($CDCl_3$, δ): 24.6, 23.6; EA: Calcd.: C 45.26, H 8.06, N 3.20, S 18.31; found: C 43.40, H 8.12, N 3.16, S 18.29.

P2$_1$P3$_1$: ^{1}H NMR ($CDCl_3$, δ): 2.85 – 2.76 (m, 2H, C$\underline{H}_2$-CH_2-CN), 2.73 – 2.61 (m, 4H, C$\underline{H}_2$-S-CH_2-C$\underline{H}_2$-CN), 2.58 – 2.48 (m, 4H, C$\underline{H}_2$-S-C$\underline{H}_2$-Pr), 1.60 –1.51 (m, 2H, C$\underline{H}_2$-CH_2-CH_3), 1.46 – 1.35 (m, 2H, C$\underline{H}_2$-CH_3), 0.98 – 0.85 (m, 7H, Si-C$\underline{H}_2$-, CH_2-C$\underline{H}_3$). 0.15 (s, 6H, Si-C$\underline{H}_3$); ^{13}C NMR ($CDCl_3$, δ): 118.6, 31.9, 31.8, 27.7, 26.8, 26.4, 22.2, 19.1, 18.4, 18.2,13.8, 0.1; ^{29}Si NMR ($CDCl_3$, δ): 24.6, 23.7; EA: Calcd.: C 44.66, H 7.78, N 4.01, S 18.34; found: C 42.59, H 7.95, N 3.76, S 18.36.

P2$_4$P3$_6$: ^{1}H NMR ($CDCl_3$, δ): 2.85 – 2.77 (m, 12H, C$\underline{H}_2$-CH_2-CN), 2.73 – 2.63 (m, 24H, C$\underline{H}_2$-S-CH_2-C$\underline{H}_2$-CN), 2.59 – 2.49 (m, 16H, C$\underline{H}_2$-S-C$\underline{H}_2$-Pr), 1.60 –1.51 (m, 8H, C$\underline{H}_2$-CH_2-CH_3), 1.46 – 1.35 (m, 8H, C$\underline{H}_2$-CH_3), 0.97 – 0.86 (m, 32H, Si-C$\underline{H}_2$-, CH_2-C$\underline{H}_3$). 0.16 (s, 30H, Si-C$\underline{H}_3$); ^{13}C NMR ($CDCl_3$, δ): 118.7, 31.9, 31.8, 27.7, 26.8, 26.5, 22.2, 19.2, 18.4, 18.3, 13.9, 0.1; ^{29}Si NMR ($CDCl_3$, δ): 24.2, 23.4; EA: Calcd.: C 44.04, 7.51. N 4.82, S 18.37; found: C 42.03, H 7.65, N 4.65, S 17.60.

P2$_3$P3$_7$: ^{1}H NMR ($CDCl_3$, δ): 2.85 – 2.78 (m, 14H, C$\underline{H}_2$-CH_2-CN), 2.73 – 2.64 (m, 28H, C$\underline{H}_2$-S-CH_2-C$\underline{H}_2$-CN), 2.58 – 2.49 (m, 12H, C$\underline{H}_2$-S-C$\underline{H}_2$-Pr), 1.60 –1.52 (m, 6H, C$\underline{H}_2$-CH_2-CH_3), 1.46 – 1.36 (m, 6H, C$\underline{H}_2$-CH_3), 0.97 – 0.87 (m, 41H, Si-C$\underline{H}_2$-, CH_2-C$\underline{H}_3$). 0.17 (s, 30H, Si-C$\underline{H}_3$); ^{13}C NMR ($CDCl_3$, δ): 118.7, 31.9, 31.8, 27.7, 26.8, 26.5, 22.2, 19.2, 18.4, 18.3, 13.9, 0.1; ^{29}Si NMR ($CDCl_3$, δ): 24.2, 23.2; EA: Calcd.: C 43.43, H 7.23, N 5.63, S 18.4; found: C 41.17, H 6.49, N 5.77, S 16.61.

P3: ^{1}H NMR ($CDCl_3$, δ): 2.85 – 2.78 (m, 2H, C$\underline{H}_2$-CH_2-CN), 2.72 – 2.64 (m, 4H, C$\underline{H}_2$-S-CH_2-C$\underline{H}_2$-CN), 0.95 – 0.88 (m, 2H, Si-C$\underline{H}_2$-), 0.18 (s, 3H, Si-C$\underline{H}_3$); ^{13}C NMR ($CDCl_3$, δ): 118.8, 27.5, 26.6, 19.0, 18. 0.0; ^{29}Si NMR ($CDCl_3$, δ): 24.2; EA: Calcd.: C 41.58, H 6.40, N 8.08, S 18.5; found C 39.47, H 6.49, N 8.04, S 17.63.

The deviations of the data from combustion analysis with the calculated ones for some of the samples is likely due to some residual solvents that were difficult to remove from the highly viscous polymers. For the amount of methanol left in the samples, see Table 1.

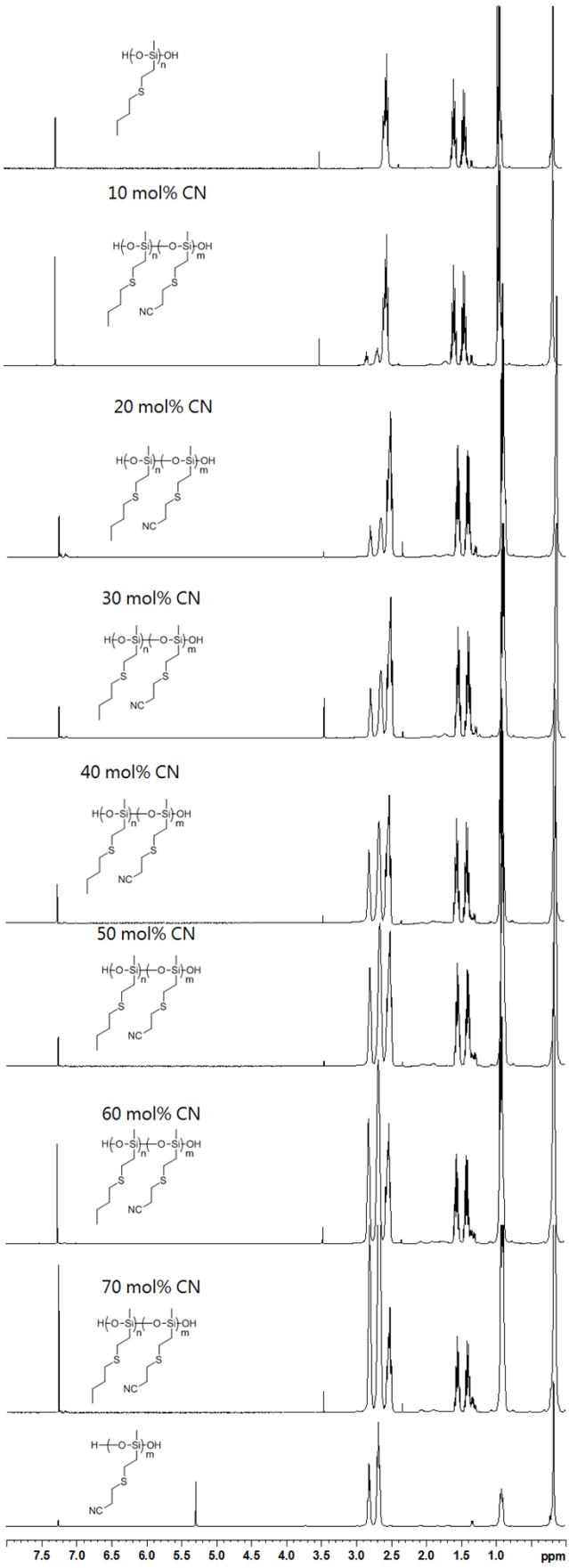

Fig. S1a ^{1}H NMR spectra of **P2**, **P3**, and **P2$_x$P3$_y$**.

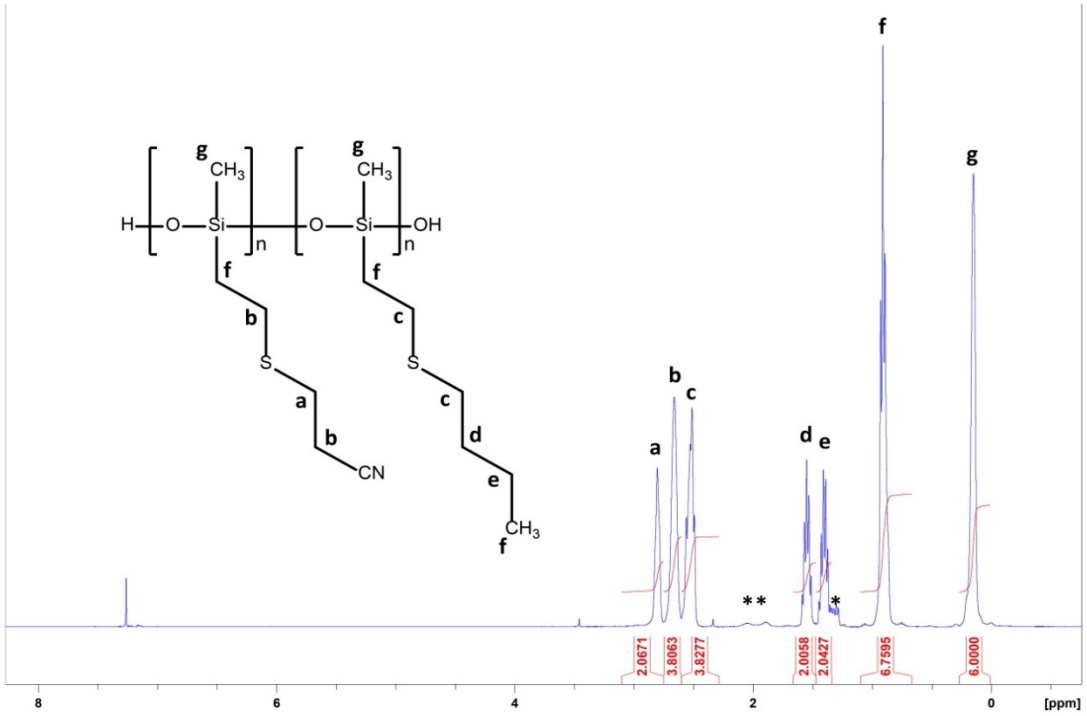

Fig. S1b ^{1}H NMR spectrum of **P2$_1$P3$_1$** with assignment of the peaks to the corresponding protons. Peaks denominated with an * are assigned to the Markovnikov addition product.

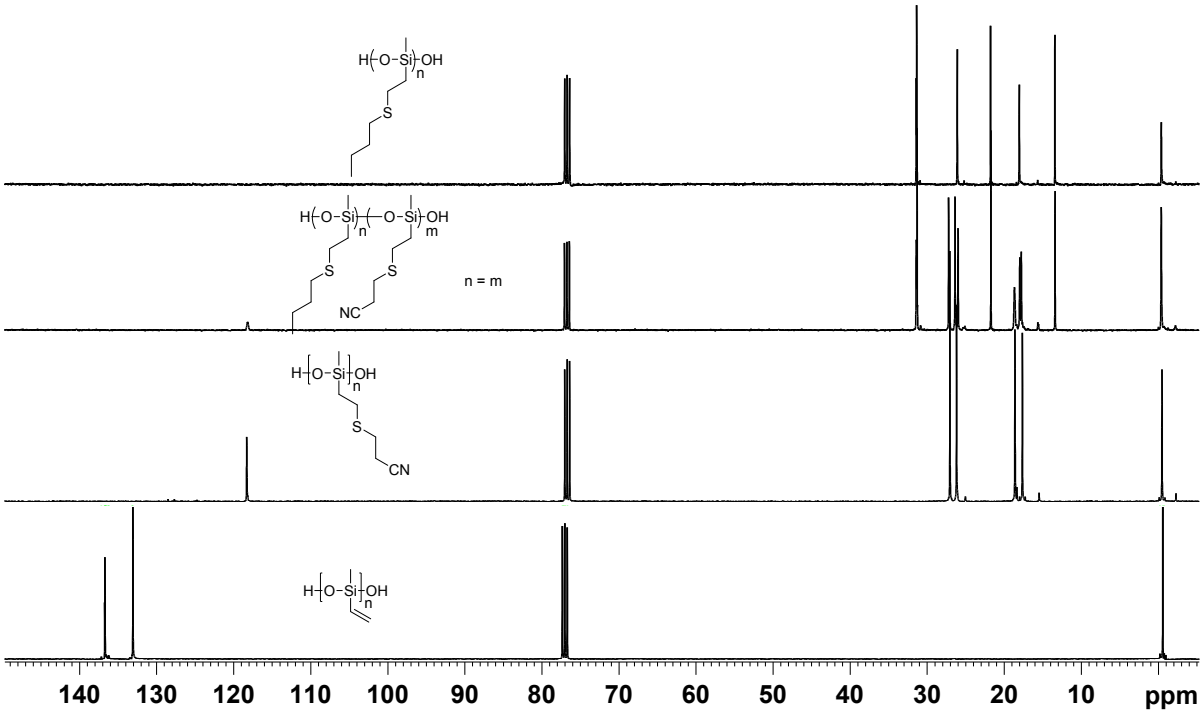

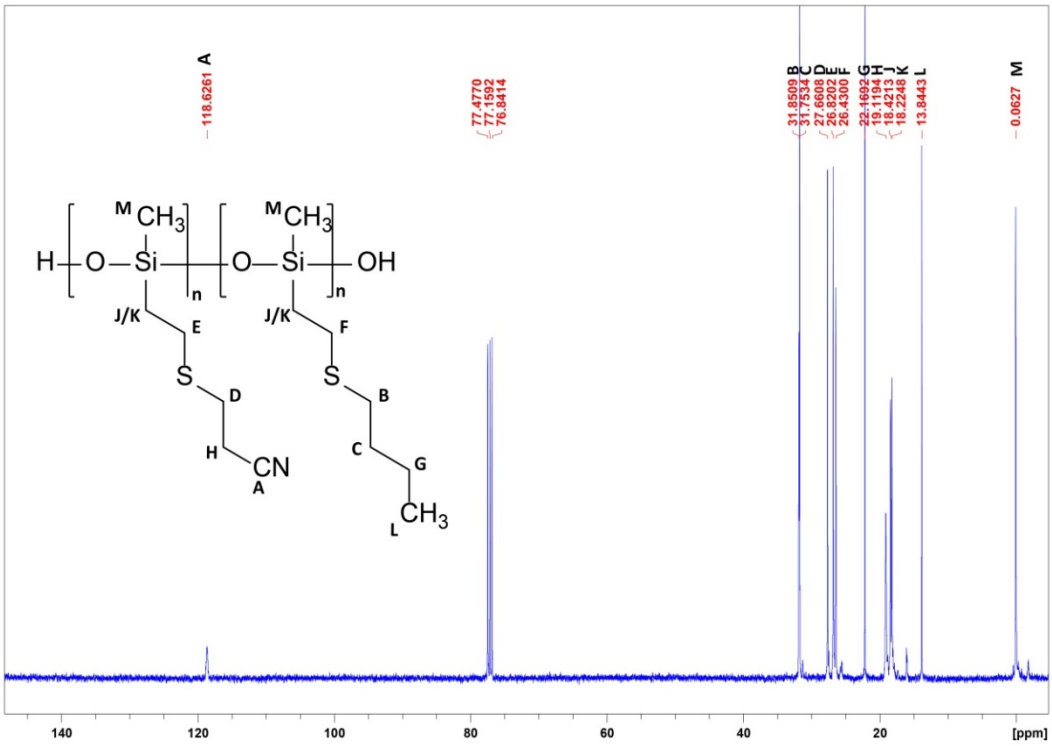

Fig. S2 ^{13}C NMR spectra of **P1**, **P2**, **P3** and **P2$_1$P3$_1$** (top) and of **P2$_1$P3$_1$** with assignment of the peaks(bottom).

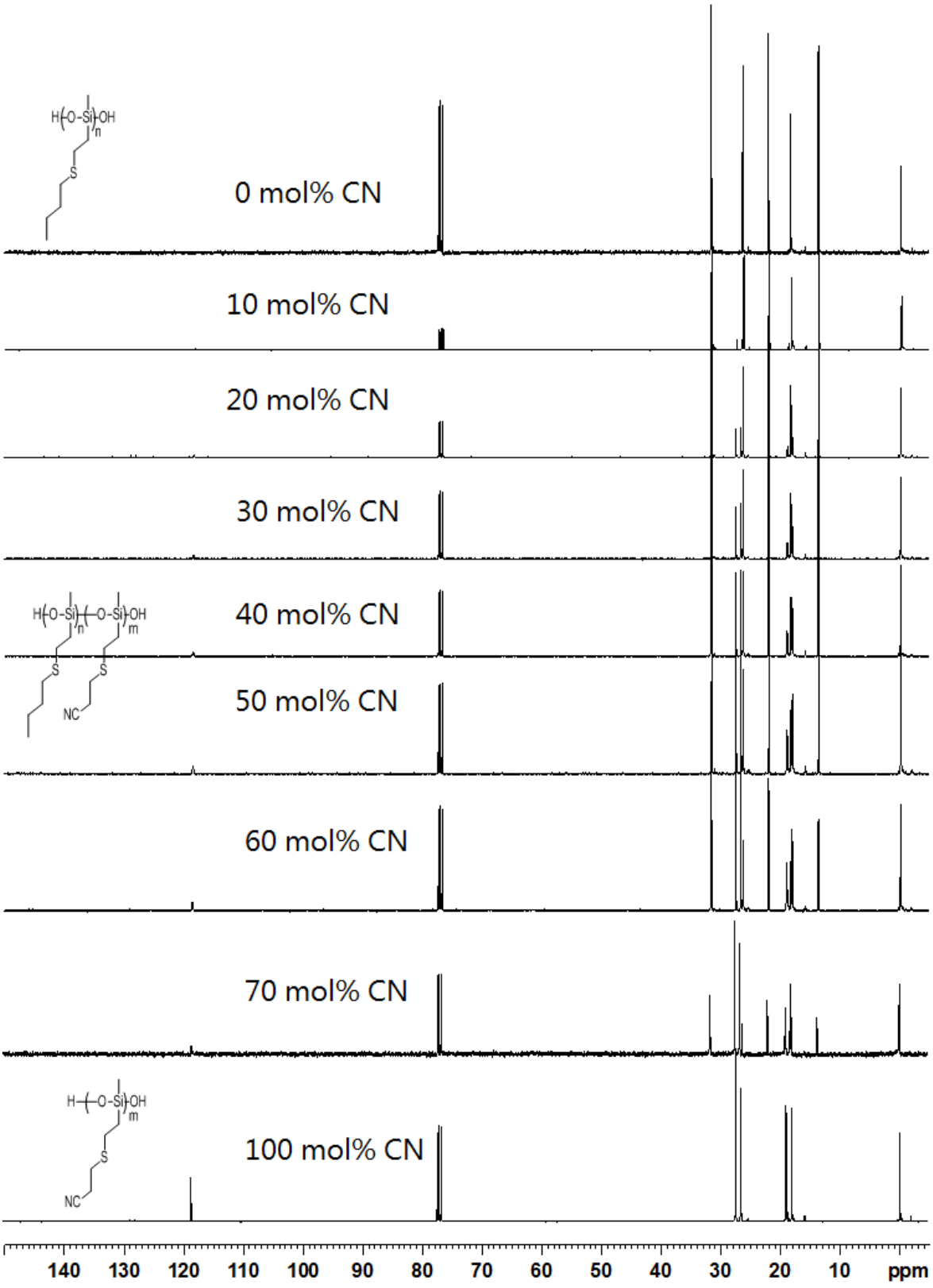

Fig. S3 ^{13}C NMR spectra of **P2**, **P3**, and **P2$_x$P3$_y$**.

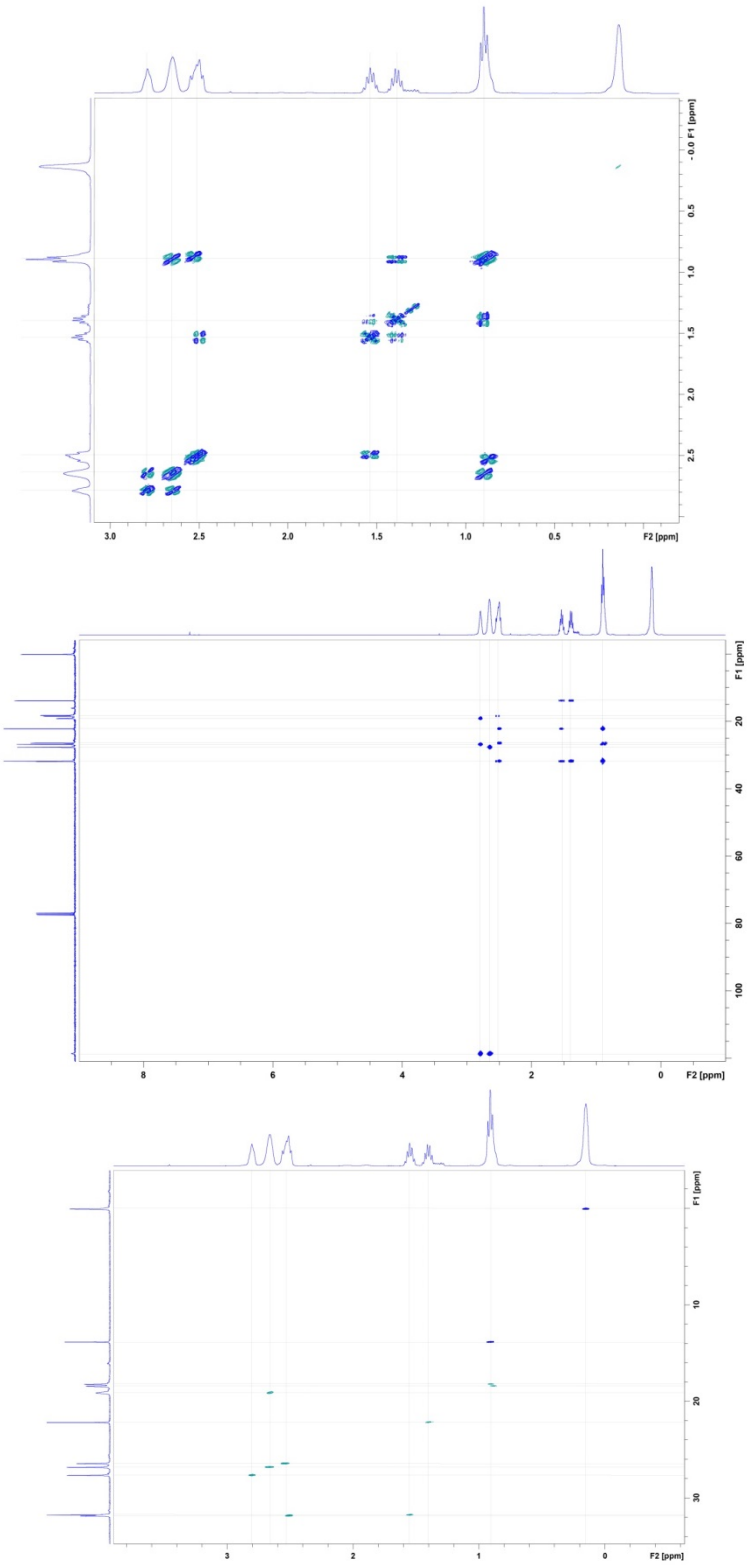

Fig. S4 ^{1}H-^{1}H-DQF-COSY NMR spectrum of $\mathbf{P2_1P3_1}$ (top); ^{1}H-^{13}C-HMBC NMR spectrum of $\mathbf{P2_1P3_1}$ (middle); ^{1}H-^{13}C-HSQC NMR spectrum of $\mathbf{P2_1P3_1}$ (bottom).

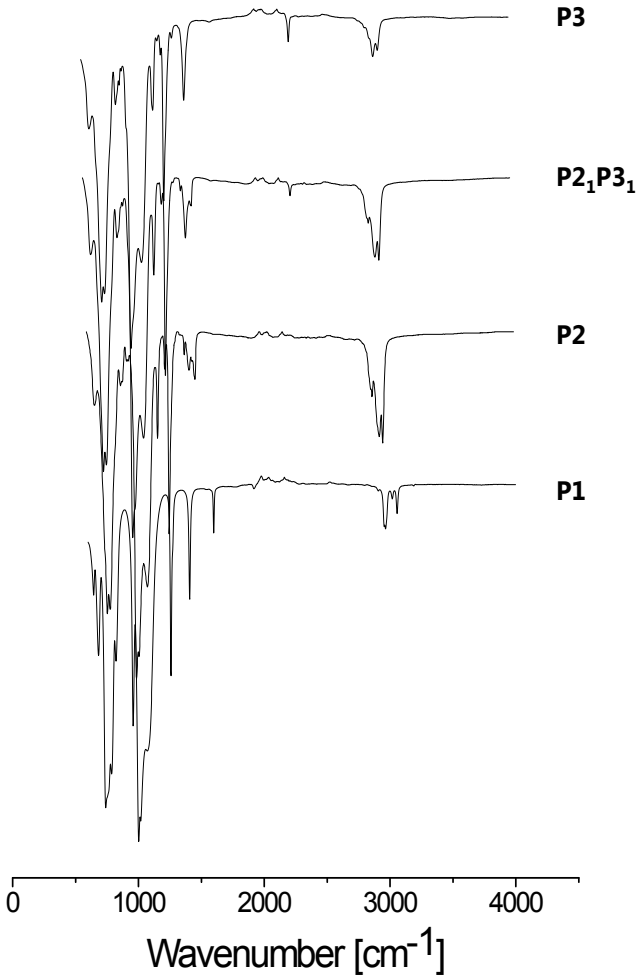

Fig. S5 The IR spectra of P**1**, **P2**, **P2$_1$P3$_1$**, and **P3**.

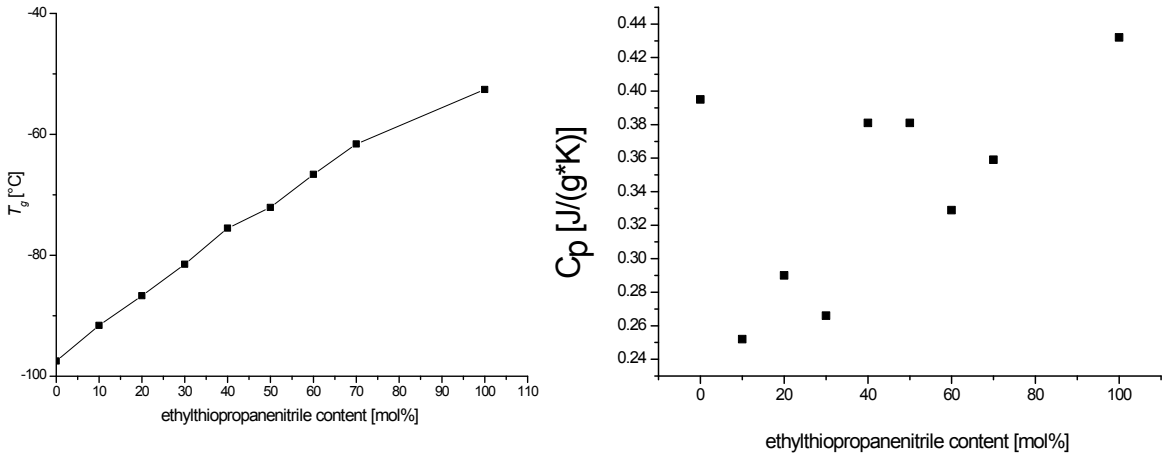

Fig. S6 The glass transition temperatures of **P2**, **P3**, **P2$_x$P3$_y$** (left). A linear increase in the T_g with increasing the amount of nitrile groups was observed. Cp of **P2**, **P3**, **P2$_x$P3$_y$** as function of mol% of polar nitrile group (right).

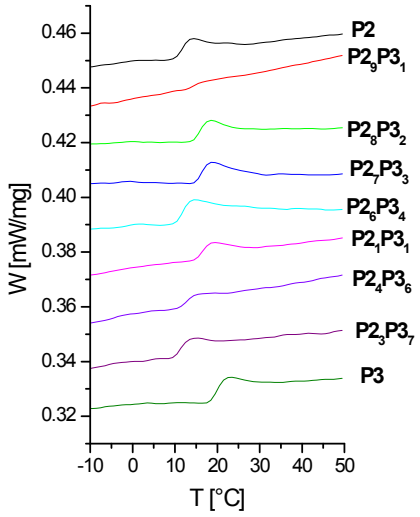

Fig. S7 The enlargement of the DSC heating scans in the melting region of the crystalline domains of **P2**, **P3** and **P2$_x$P3$_y$**.

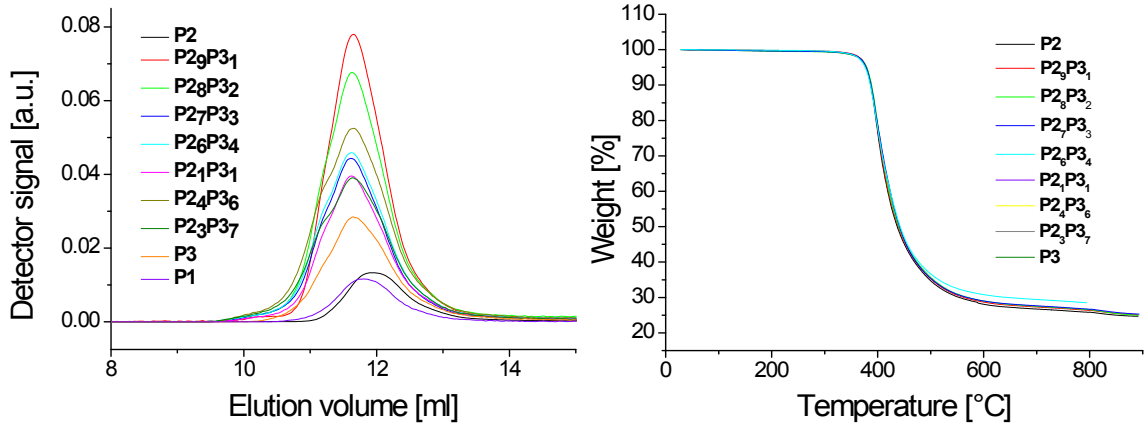

Fig. S8 GPC elugrams in tetrahydrofurane (left) and TGA (right) of **P2**, **P3**, and **P2$_x$P3$_y$**. The elugrams of **P2**, **P3**, and **P2$_x$P3$_y$** were integrated from 10.5 ml to 13.5 ml.

A composition of up to four Havriliak-Negami functions [Havriliak, S. & Negami, S. *Polymer,* **1967**, *8*, 161] for the α-relaxation (segmental motion) in the amorphous phase, the alpha-relaxation of segments neighbouring crystalline domains and the local fluctuations of the methyl- and nitrile-terminated side chains, respectively (each accounted for by the index *j* in the following equetion) and a term accounting for conductivity [Kremer, F. & Schönhals, A. *(Eds.)* Broadband Dielectric Spectroscopy *Springer, Berlin Heidelberg,* **2003**] has been employed to fit the dielectric loss spectra $\varepsilon''(f)$

$$\varepsilon''(\omega) = \sum_{j=1}^{4} -\mathrm{Im}\left(\frac{\Delta\varepsilon_j}{\left(1 + i\left(\omega\tau_{HN,j}\right)^{\alpha_j}\right)^{\beta_j}} \right) + \frac{a\sigma_{DC}}{\varepsilon_0\omega^s} \qquad \text{Equation S1}$$

with the angular frequency $\omega=2\pi f$, the symbol for the imaginary part Im and the imaginary unit $i=(-1)^{0.5}$. Four parameters describe the imaginary part of the Havriliak-Negami function: the dielectric relaxation strength $\Delta\varepsilon$, the relaxation time τ_{HN} and the parameters for symmetric and asymmetric broadening α and β, respectively. The conductivity contribution consists of the DC-conductivity σ_{DC}, the exponent s ($0<s\leq1$) and the parameter $a=(1\ \mathrm{Hz})^{s-1}$ to correct for the units. ε_0 denotes the permittivity of the vacuum. Note that for fitting each single temperature, only those components (number of Havriliak-Negami functions, conductivity contribution) which are present in the respective loss spectrum were included in the composed fit function.

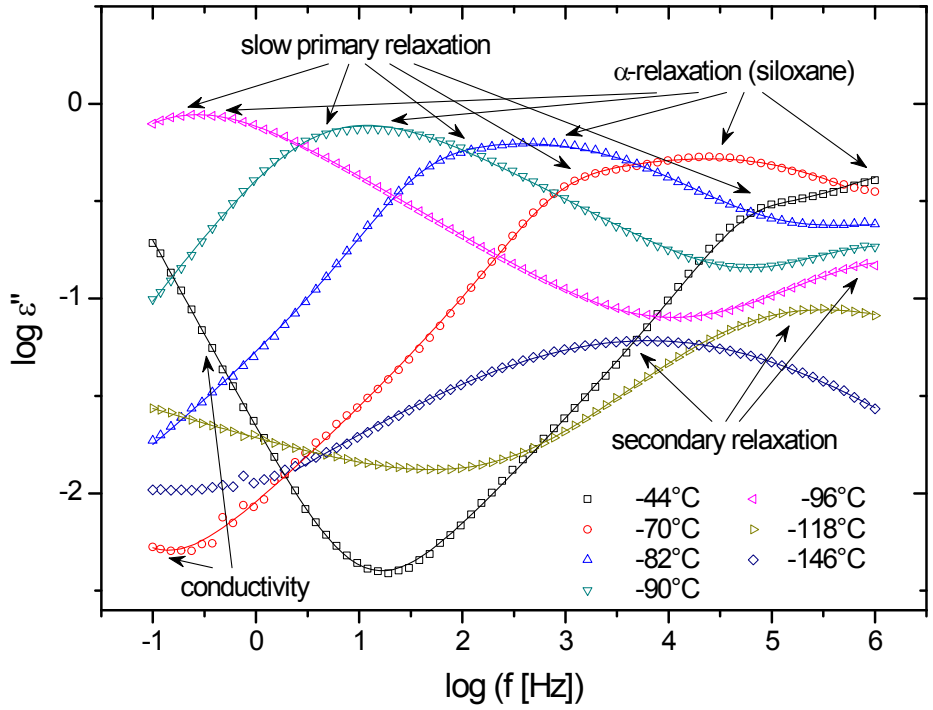

Fig. S9 Dielectric loss as a function of frequency of polymer **P2** at different temperature as indicated. Solid lines represent fits of equation 1 to the data.

The mean relaxation time τ indicating the peak position in the spectra can be calculated from the relaxation time τ_{HN} and the parameters for symmetric and asymmetric broadening α and β extracted from Equation S1

$$\tau = \tau_{HN}\left(\frac{\sin\left(\frac{\beta\gamma\pi}{2+2\gamma}\right)}{\sin\left(\frac{\beta\pi}{2+2\gamma}\right)}\right)^{1/\beta} \qquad \text{Equation S2}$$

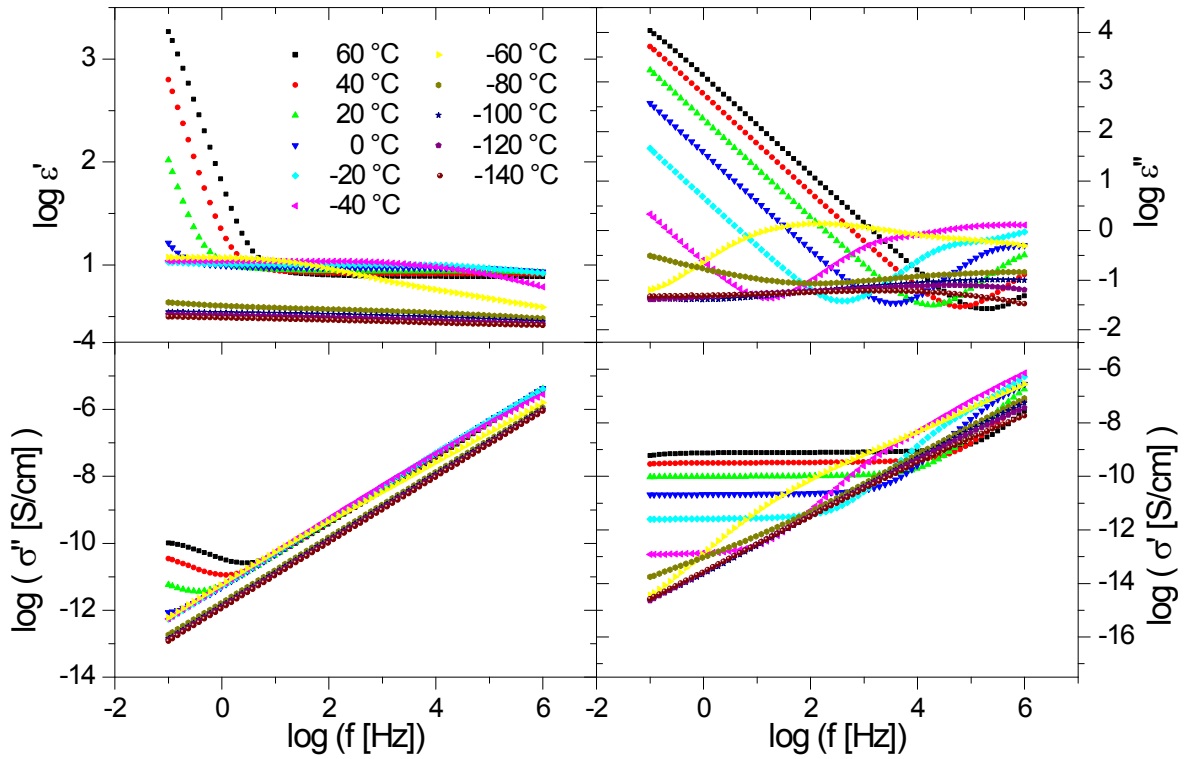

Fig. S10 Dielectric permittivity (ε') and loss (ε") as well as the real and imaginary part of the complex conductivity (σ' and σ", respectively) of the sample **P2$_1$P3$_1$** as a function of frequency for different temperatures as indicated.

To analyze the temperature dependence of the mean relaxation rates, two equations were employed. First, primary relaxations (the α-relaxations) follow the Vogel-Fulcher-Tammann equation [Vogel, H. *Physikalische Zeitschrift,* **1921***, 22*, 645; Fulcher, G. S. *Journal of the American Chemical Society,* **1925***, 8*, 339; Tammann, G. & Hesse, G. *Zeitschrift für anorganische und allgemeine Chemie,* **1926***, 156*, 245] which is characteristic for glassy systems

$$\tau(T) = \tau_0 \exp\left(\frac{DT_0}{T - T_0}\right) \qquad \text{Equation S3}$$

with the relaxation relaxation time in the infinite temperature limit τ_0, the so-called fragility parameter D and the Vogel temperature T_0.

Second, the secondary relaxations, i.e. local fluctuations of side chains, typically exhibit a thermal activation $\tau(T)$ according to the Arrhenius equation

$$\tau(T) = \tau_0 \exp\left(\frac{E_A}{RT}\right) \qquad \text{Equation S4}$$

where τ_0 denotes the relaxation time in the infinite temperature limit, E_A the activation energy and R=8.314 J(mol K)$^{-1}$ the universal gas constant.

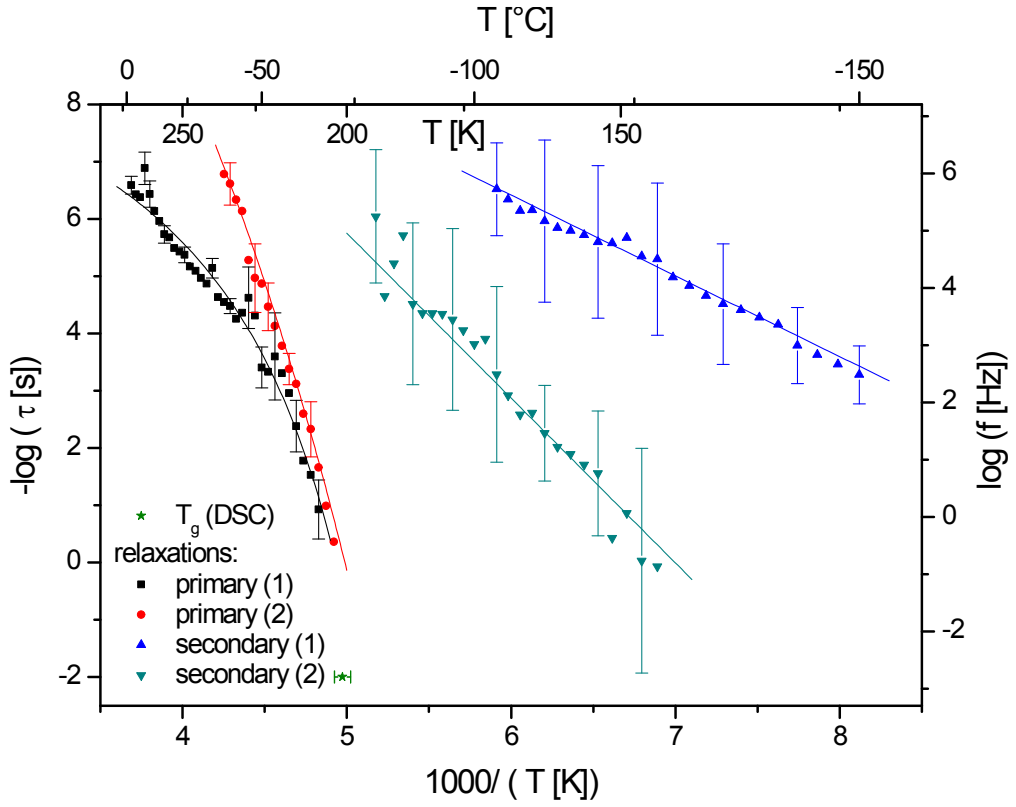

Fig. S11 Activation plot of the mean relaxation times τ extracted from the dielectric loss spectra (Fig. S9) of sample **P2$_1$P3$_1$**. Two primary relaxations can be identified according to their Vogel-Fulcher-Tammann temperature dependence (Equation S3), which coincide with the calorimetric glass transition as determined by DSC, as well as a secondary relaxation which exhibits an Arrhenius type activation (Equation S4). The error bars indicate the uncertainty of the fit parameters; in the primary relaxations, this uncertainty is larger due to the proximity of these two processes.

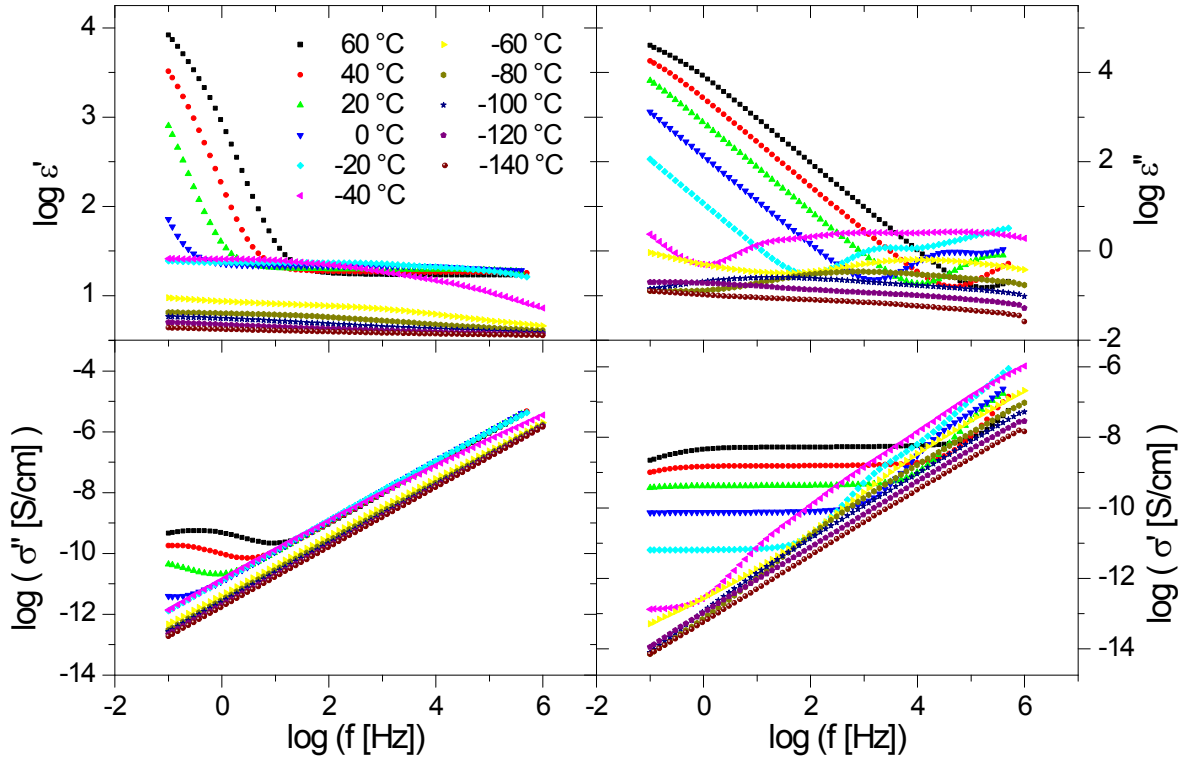

Fig. S12 Dielectric permittivity (ε') and loss (ε") as well as the real and imaginary part of the complex conductivity (σ' and σ", respectively) of the sample **P3** as a function of frequency for different temperatures as indicated.

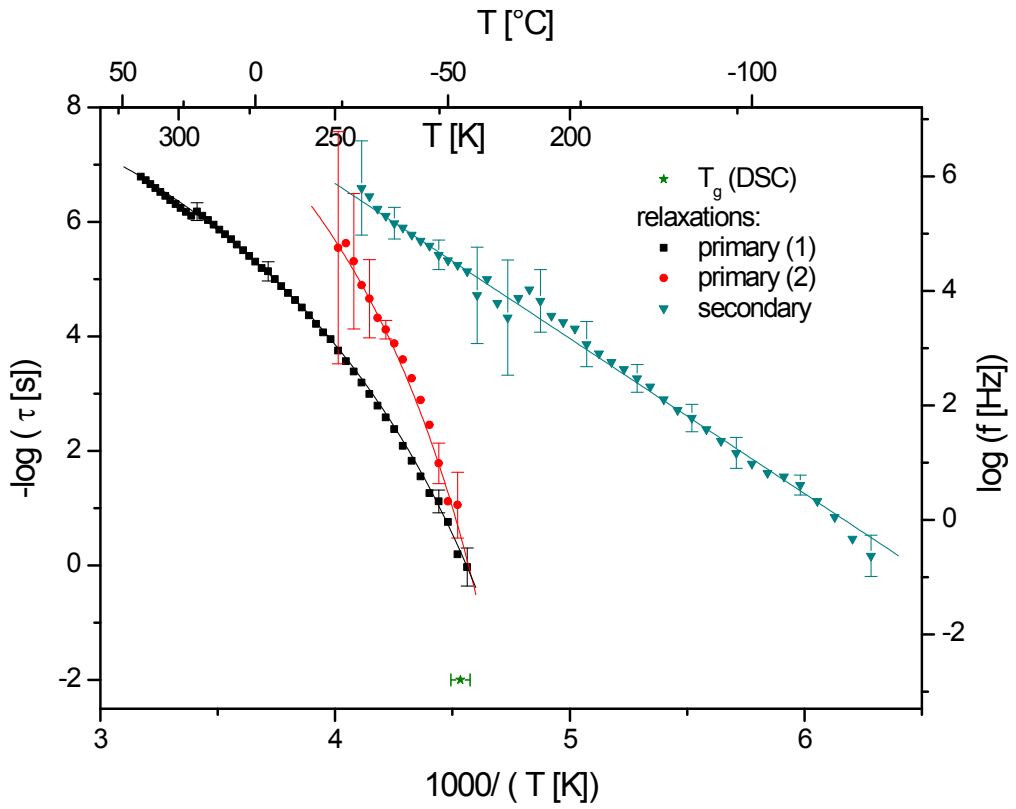

Fig. S13 Activation plot of the mean relaxation times τ extracted from the dielectric loss spectra (Fig. S12) of sample **P3**. Two primary relaxations can be identified according to their Vogel-Fulcher-Tammann temperature dependence (Equation S3), which coincide with the calorimetric glass transition as determined by DSC, as well as a secondary relaxation which exhibits an Arrhenius type activation (Equation S4). The error bars indicate the uncertainty of the fit parameters; in the primary relaxations, this uncertainty is larger due to the proximity of these two processes.

Table S1 VFT fit parameters of the α-relaxation of the siloxane backbone and the slower primary relaxation of unclear origin according to Equation S3. For the amorphous α-relaxation, also the expected glass transition temperature T_g is given by extrapolating the VFT fit to a mean relaxation time of τ=100s.

	α-relaxation (amorphous)				slower primary relaxation		
sample	τ_0 [s]	D	T_0 [K]	T_g [°C]	τ_0 [s]	D	T_0 [K]
PDMS	2 (±9) 10^{-17}	13.7 (±4.9)	109 (±7)	-129 (±25)	1 (±11) 10^{-7}	2.4 (±3.8)	135 (±21)
P2	1.9 (±1.8) 10^{-12}	5.6 (±0.7)	146 (±2)	-101 (±7)	7.6 (±8.9) 10^{-11}	8.1 (±2.0)	128 (±7)

P2$_1$P3$_1$	7 (±73) 10^{-23}	31 (±20)	124 (±21)	-78 (±91)	4.6 (±6.4) 10^{-10}	4.0 (±1.1)	171 (±7)
P3	1.7 (±6.6) 10^{-13}	6.3 (±2.6)	180 (±9)	-60 (±28)	2.8 (±0.6) 10^{-11}	7.8 (±0.3)	166 (±1)

Table S2 Arrhenius fit parameters of the local fluctuations of the methyl-terminated and the nitrile-terminated side chains, respectively according to Equation S4.

sample	terminal group	τ_0 [s]	E_A [kJ/mol]
P2	methyl	7.0 (±0.6) 10^{-15}	23.2 (±0.1)
P2$_1$P3$_1$	methyl	1.3 (±0.9) 10^{-15}	27.0 (±0.7)
P2$_1$P3$_1$	nitrile	7 (±15) 10^{-21}	55.1 (±3.1)
P3	nitrile	3.2 (±0.6) 10^{-18}	51.8 (±0.3)

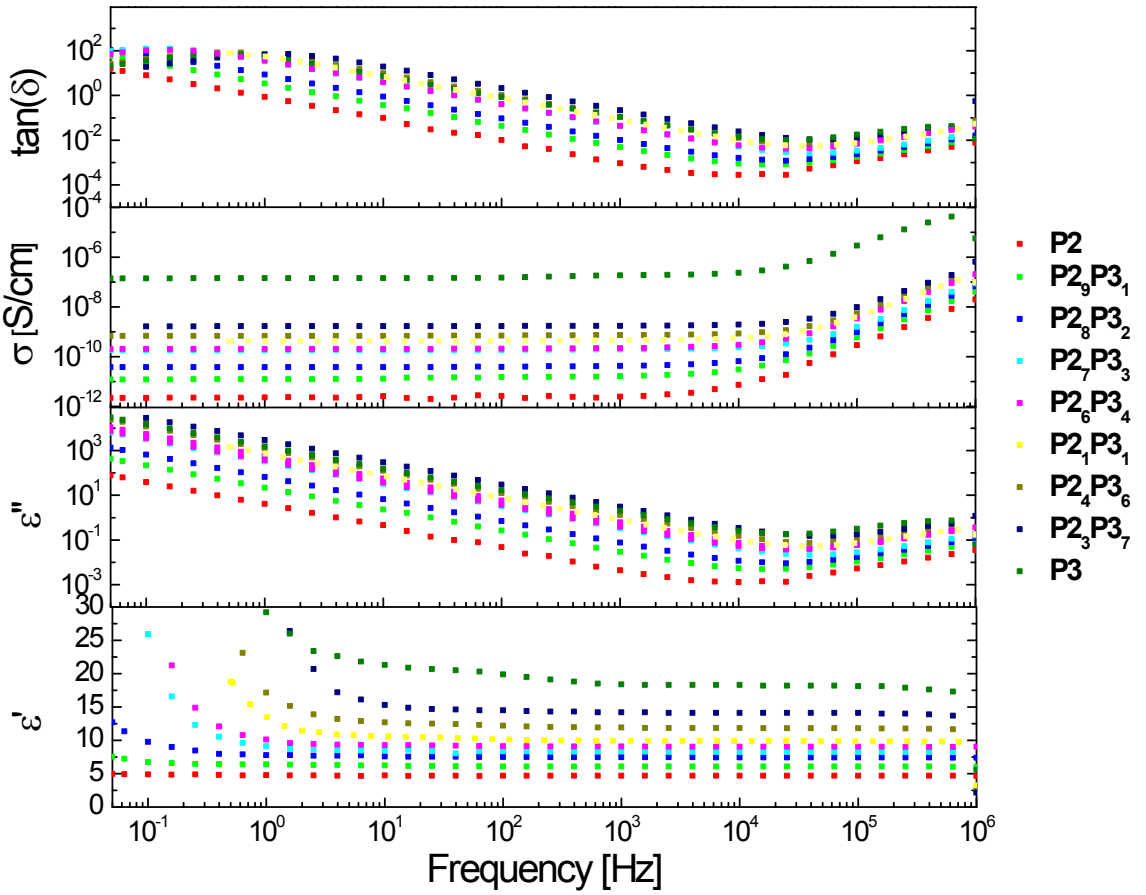

Fig. S14 Dielectric properties: permittivity (ε'), dielectric loss (ε''), conductivity (σ), loss factor ($tan\ \delta$) of polymers **P2**, **P3** and **P2$_x$P3$_y$**.

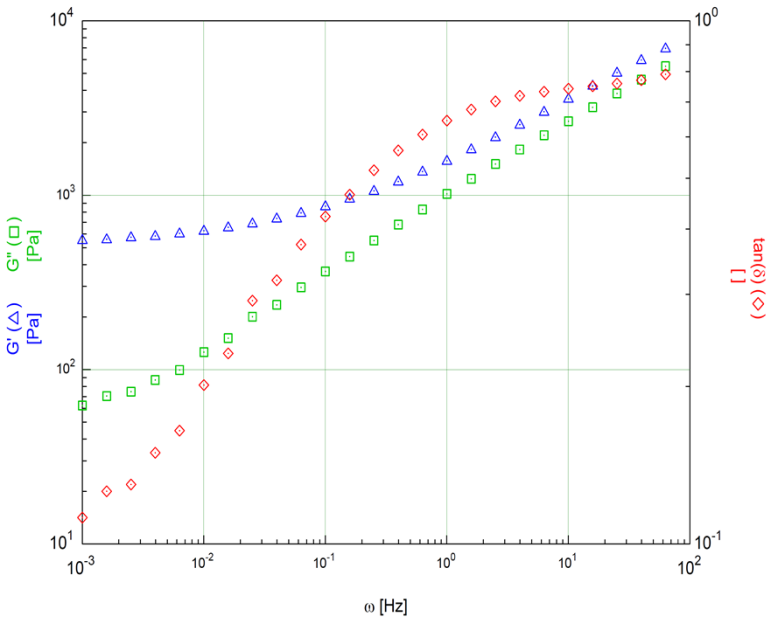

Fig. S15 Dependence of the real part (G') and imaginary (G'') parts of the shear modulus and the loss angle tan (δ) for a material prepared by cross-linking **P3** as a function of frequency and room temperature.

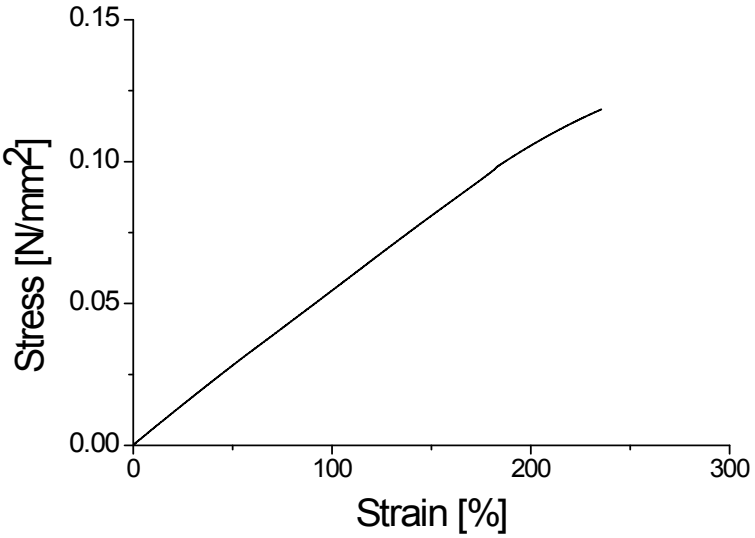

Fig. S16 Stress-strain curves of an elastomer prepared starting from **P3** by crosslinking *via* the hydroxyl end-groups.